Phase transformations in slit-pores: the role of metastable phases

2002 J. Phys.: Condens. Matter 14 5673

(http://iopscience.iop.org/0953-8984/14/23/303)

INSTITUTE OF PHYSICS PUBLISHING JOURNAL OF PHYSICS: CONDENSED MATTER

J. Phys.: Condens. Matter **14** (2002) 5673–5697 PII: S0953-8984(02)33698-1

Phase transformations in slit-pores: the role of metastable phases

Sabine H L Klapp, Henry Bock[1], Dennis J Diestler[2] and Martin Schoen[3]

Stranski-Laboratorium für Physikalische und Theoretische Chemie, Sekretariat TC7, Technische Universität Berlin, Straße des 17. Juni 124, D-10623 Berlin, Germany

E-mail: klapp@terra.chem.tu-berlin.de, hbock@unity.ncsu.edu, ddiestler1@unl.edu and martin@terra.chem.tu-berlin.de

Received 12 February 2002
Published 30 May 2002
Online at stacks.iop.org/JPhysCM/14/5673

Abstract

The behaviour of metastable phases involved in phase transformations of a simple fluid confined to a nanoscopic slit-pore is investigated within the mean-field lattice-gas approximation. For small displacements $\delta\rho_i$ (where i labels lattice sites) of local densities about their values ρ_i^0 at the (metastable) minima of the grand potential functional $\Omega[\boldsymbol{\rho}]$, the change in Ω is quadratic in $\delta\rho_i$. The 'force constants' associated with the $\delta\rho_i$ are the elements of the Hessian evaluated at the minimum (i.e., $(\partial^2\Omega/\partial\rho_i\,\partial\rho_j)_0$). If the walls of the pore are homogeneous, the Hessian reduces, in reciprocal space, to a single $n_z \times n_z$ matrix, where n_z is the number of lattice planes parallel with the walls. The complete phase diagram, including spinodals, is determined for $n_z = 3$, in which case the Hessian can be diagonalized explicitly. As the spinodal of a given (metastable) phase is approached, a characteristic eigenvalue of the Hessian tends to zero. The components of the corresponding eigenvector, which are proportional to homogeneous density fluctuations in the lattice planes, can indicate the nascent phase to which the metastable phase is transforming. The new phase is not necessarily the globally stable one. This suggests that sorption could take place via stepwise transformations involving phases that are metastable on the timescale of the observation.

[1] Present address: Department of Chemical Engineering, North Carolina State University, Raleigh, NC 27695-7905, USA.
[2] Permanent address: Department of Agronomy and Horticulture, University of Nebraska–Lincoln, Lincoln, NE 68583-0915, USA.
[3] Author to whom any correspondence should be addressed.

0953-8984/02/235673+25$30.00

1. Introduction

First-order phase transitions normally take place via metastable states. A classic example is the gas–liquid transition at a temperature below critical [1]. In order to observe condensation in a very pure sample of a gas on a 'reasonable' timescale, one must typically raise the pressure of the gas considerably above the value at which the gas is in thermodynamic equilibrium with liquid at the given temperature. For the metastable gas to condense, clusters (i.e., microscopic regions of liquid) of a 'critical' size must form. Visible droplets result from rapid growth of critical clusters through a succession of collisions with single molecules in the surrounding metastable gas. The rate of droplet formation is thus controlled by the population of critical clusters, which increases markedly with the degree of supersaturation of the metastable gas. Other classic examples of phase transformations involving metastable states come readily to mind: boiling of superheated liquid, crystallization of a pure supercooled liquid, and precipitation of a dissolved solid from a supersaturated solution. In all cases, the course of the transition consists in the creation and subsequent growth of nuclei of the new (stable) phase in the presence of the existing metastable phase. The rate of appearance of the new phase is determined by the steady population of clusters of critical size [2–4].

Over the past few years we have been studying phase equilibria of 'simple' fluids confined to slit-pores with chemically heterogeneous walls [5–9]. Walls possessing quite simple patterns (i.e., weakly and strongly adsorbing stripes that alternate periodically in one transverse direction) can give rise to confined phases having surprisingly diverse morphologies: droplets, vesicles, liquid bridges in addition to the 'normal' gas and liquid phases. We have also examined the role played by nanoscopic liquid bridges in static friction [10]. Metastable states involving these and similar new morphologically distinct phases could be responsible for hysteresis observed in experiments on sorption [11] and friction [12]. The kinetics of phase transformations in which new morphologies participate is consequently of great interest to us. Any such transitions presumably proceed by formation and growth of critical clusters of the new (stable) phase in the presence of the metastable one. In contrast to nucleation in homogeneous phases, however, one must now account for heterogeneity of the confined phase [13–17]. From a theoretical viewpoint this is a daunting prospect. Before possible mechanisms of cluster formation can be treated, however, one needs to know the complete phase diagram of the system, including not only lines of coexistence but also limits of existence of metastable phases, i.e. the spinodals.

One of the purposes of this article is to present such a complete phase diagram for the slit-pore with chemically *homogeneous* walls, which is obviously a special case of chemically heterogeneous walls. A numerical procedure for determination of the equilibrium phase diagram has been developed and applied within the context of the nearest-neighbour lattice-gas model [18], which yields a satisfactory semiquantitative description [8]. In the present work we focus on a new approach to locating the spinodals. The previously developed numerical technique yields the *minima* of the grand potential functional $\Omega[\boldsymbol{\rho}]$ of the local density $\boldsymbol{\rho} = \{\rho_1, \rho_2, \ldots, \rho_{\mathcal{N}}\}$ on the $\mathcal{N}$ sites of the lattice. For any given thermodynamic state (specified by the chemical potential μ, absolute temperature T, and such additional model parameters as the (discrete) distance n_z between the walls and the details of the chemical pattern which govern the interaction between fluid molecules and the walls), in the vicinity of a first-order phase transition $\Omega[\boldsymbol{\rho}]$ exhibits several minima, the lowest of which corresponds to the globally stable state. Other minima refer to metastable states. To locate the spinodals we expand Ω up to second order in displacements $\delta\boldsymbol{\rho}$ of the local density about the density $\boldsymbol{\rho}^0$ at the (metastable) minimum. This yields a quadratic expression for the change $\delta\Omega = \Omega[\boldsymbol{\rho}] - \Omega[\boldsymbol{\rho}^0]$ in the grand potential functional due to displacements in the $\mathcal{N}$ possible

'directions' in $\boldsymbol{\rho}$-space. The Hessian matrix elements $H_{ij} \equiv (\partial^2\Omega/\partial\rho_i\,\partial\rho_j)_0$ evaluated at the minimum correspond to effective 'force constants' associated with the displacements. The $\mathcal{N}$ normal modes and corresponding eigenvalues $\{\lambda_i, i = 1, 2, \ldots, \mathcal{N}\}$ can be obtained, in principle, by diagonalizing the Hessian. The eigenvalue λ_i is the force constant associated with the ith normal mode, which consists of a *concerted* displacement of all $\mathcal{N}$ components of $\boldsymbol{\rho}$. As the state of the system approaches a spinodal, the eigenvalue λ_d associated with a 'dominant' mode becomes small, indicating that the mode becomes soft (i.e., the restoring force becomes small). At the spinodal $\lambda_d = 0$, the minimum becomes a *saddle point* and the state becomes unstable. The dominant normal mode can provide information about the *direction* of the phase transformation in $\boldsymbol{\rho}$-space.

In section 2 we describe the model system and determination of its phase diagram. Section 3.1 is devoted to an outline of the general approach to location of spinodal lines. This would seem to require diagonalization of an $\mathcal{N} \times \mathcal{N}$ matrix, which is clearly out of the question for large $\mathcal{N}$. However, in section 3.2 we show how translational symmetry in planes parallel with the walls (in the case of chemically homogeneous walls) can be exploited to reduce greatly the dimension of the Hessian. This is achieved by representing the Hessian in reciprocal space by means of a discrete Fourier transform. In reciprocal space the Hessian assumes block-diagonal form: a set of real, symmetric $n_z \times n_z$ matrices $\tilde{\mathbf{H}}(\boldsymbol{k})$, each one corresponding to a particular value of the reciprocal vector $\boldsymbol{k}$. Section 3.3 deals with the special situation of principal interest to us, namely that only nearest neighbours interact. In this case, $\tilde{\mathbf{H}}(\boldsymbol{k})$ can be decomposed into a $\boldsymbol{k}$-independent matrix $\tilde{\mathbf{H}}'$ and the identity matrix multiplied by a scalar function of $\boldsymbol{k}$. As a consequence, only a single diagonalization of $\tilde{\mathbf{H}}'$ is required to obtain *all* the eigenvalues and eigenvectors. In section 3.4 we present an analysis of the density–density response function, deriving in closed form its asymptotic dependence on the distance between lattice sites.

Section 4 is devoted to a detailed analysis of the homogeneous slit-pore within the nearest-neighbour mean-field lattice-gas approximation. The (reduced) thermodynamic state parameters comprise μ/ϵ_{ff}, k_BT/ϵ_{ff} (k_B Boltzmann's constant), n_z, and $\epsilon_{fw}/\epsilon_{ff}$, where ϵ_{ff} and ϵ_{fw} are the respective magnitudes of the fluid–fluid and fluid–wall attraction. Complete phase diagrams are determined for a narrow pore ($n_z = 3$) with strongly attractive walls ($\epsilon_{fw}/\epsilon_{ff} = 1.9$). The eigenvalues and eigenvectors of $\tilde{\mathbf{H}}$ are obtained explicitly in terms of T and $\boldsymbol{\rho}^0(\mu, T)$. The behaviour of the eigenmodes as μ approaches the spinodals is scrutinized for several particularly interesting temperatures. The components of the dominant eigenvector can indicate the 'new' phase toward which the metastable one is tending as the state of the system approaches the spinodal.

2. Lattice-gas model of slit-pore

We begin by considering a quite general lattice model for a simple fluid confined between two plane-parallel walls that are chemically patterned so that the (equilibrium) system is periodic in both transverse directions (i.e., x- and y-directions). The positions of fluid molecules are constrained to the sites of an $n_x \times n_y \times n_z$ ($=M \times M \times n_z$) simple-cubic lattice. For simplicity we take the period to be the same in the x- and y-directions. The coordinates of a lattice site are specified by the triplet of integers (m_x, m_y, m_z). The lattice constant is set equal to the effective molecular diameter σ. Distance is then implicitly given in units of σ. The hard cores of the molecules are reflected in the restriction on the occupancy of any site to one molecule at most. For convenience, we take M to be even and the coordinates of lattice sites to run from $m = -M/2$ to $M/2$ in the x- and y-directions. Periodic boundary conditions are applied on the planes $m_x = \pm M/2$ and $m_y = \pm M/2$. The z-coordinate runs from $m_z = 1$ on the

'contact' layer of sites at the lower wall to $m_z = n_z$ on the contact layer at the upper wall. The interaction of a molecule at site i (m_x, m_y, m_z) with the 'external' field of the walls is represented by Φ_i. The potential energy of the lattice gas can therefore be expressed as

$$U(\boldsymbol{s}) = \tfrac{1}{2}\sum_{i=1}^{\mathcal{N}}\sum_{j\neq i}^{\mathcal{N}} u_{\mathrm{a}}(i,j)s_i s_j + \sum_{i=1}^{\mathcal{N}}\Phi_i s_i \tag{2.1}$$

where $\mathcal{N} = M^2 n_z$, the total number of sites, and $\boldsymbol{s} = (s_1, s_2, \ldots, s_{\mathcal{N}})$ denotes the instantaneous configuration (i.e., the ordered set of occupation numbers) such that

$$s_i = \begin{cases} 0, & \text{empty site} \\ 1, & \text{occupied site.} \end{cases} \tag{2.2}$$

In (2.1), $u_{\mathrm{a}}(i,j)$ is the potential energy of attraction between molecules occupying sites i and j. In general, $u_{\mathrm{a}}(i,j)$ depends only on the distance between the sites.

The grand potential Ω is given by

$$\Omega = -\beta^{-1}\ln\Xi \tag{2.3}$$

in terms of the grand partition function [19]

$$\Xi = \sum_{\boldsymbol{s}}\exp\left\{-\beta\left[\tfrac{1}{2}\sum_{i=1}^{\mathcal{N}}\sum_{j\neq i}^{\mathcal{N}} u_{\mathrm{a}}(i,j)s_i s_j + \sum_{i=1}^{\mathcal{N}}\mu_i s_i\right]\right\} \tag{2.4}$$

where the sum on $\boldsymbol{s}$ is over all $2^{\mathcal{N}}$ allowed states. The *local* chemical potential μ_i is defined by

$$\mu_i \equiv \Phi_i - \mu \tag{2.5}$$

and $\beta \equiv (k_{\mathrm{B}}T)^{-1}$.

Application of the Bogoliubov variational theorem [20, 21] yields the following relation for the grand potential in the mean-field approximation:

$$\Omega \leqslant \Omega[\boldsymbol{\rho}] = \mathcal{F}_{\mathrm{id}} + \mathcal{F}_{\mathrm{ex}} + \sum_{i=1}^{\mathcal{N}}\mu_i\rho_i \tag{2.6}$$

where $\mathcal{F}_{\mathrm{id}}$ and $\mathcal{F}_{\mathrm{ex}}$, respectively, the 'ideal' and 'excess' contributions to the Helmholtz free energy, are defined as

$$\begin{aligned} \mathcal{F}_{\mathrm{id}} &\equiv \beta^{-1}\sum_{i=1}^{\mathcal{N}}[\rho_i\ln\rho_i + (1-\rho_i)\ln(1-\rho_i)] \\ \mathcal{F}_{\mathrm{ex}} &\equiv \tfrac{1}{2}\sum_{i=1}^{\mathcal{N}}\sum_{j\neq i}^{\mathcal{N}} u_{\mathrm{a}}(i,j)\rho_i\rho_j. \end{aligned} \tag{2.7}$$

In (2.6), $\Omega[\boldsymbol{\rho}]$ stands for the grand potential *functional* of the *a priori* unknown mean local densities $\rho_i \equiv \langle s_i\rangle$. The best estimate of Ω and of the density (vector) $\boldsymbol{\rho} = (\rho_1, \rho_2, \ldots, \rho_{\mathcal{N}})$ is determined by minimizing $\Omega[\boldsymbol{\rho}]$, since, according to (2.6), $\Omega[\boldsymbol{\rho}]$ is an upper bound of Ω. The *necessary* condition for $\Omega[\boldsymbol{\rho}]$ to be a minimum is

$$\left(\frac{\partial\Omega[\boldsymbol{\rho}]}{\partial\rho_i}\right)_0 = 0 \qquad i = 1, 2, \ldots, \mathcal{N} \tag{2.8}$$

where the subscript 0 denotes that the partial derivatives are evaluated at $\boldsymbol{\rho}^0$. Using the defining expression for $\Omega[\boldsymbol{\rho}]$ in (2.6) and (2.7), we obtain from (2.8)

$$-\beta\left(\frac{\partial\mathcal{F}_{\mathrm{ex}}}{\partial\rho_i}\right)_0 = \ln\left(\frac{\rho_i^0}{1-\rho_i^0}\right) + \beta\mu_i. \tag{2.9}$$

This form of the condition for the minimum is convenient for the analysis carried out in section 3.4. Now using the definition of $\mathcal{F}_{\rm ex}$ in (2.7) we can recast (2.9) as

$$\beta^{-1}\ln\frac{\rho_i^0}{1-\rho_i^0}+\sum_{j\neq i}^{\mathcal{N}}u_{\rm a}(i,j)\rho_j^0+\mu_i=0 \qquad i=1,2,\ldots,\mathcal{N}. \tag{2.10}$$

Formally solving (2.10) yields, of course, all *extrema* of $\Omega[\boldsymbol{\rho}]$. However, the particular iterative procedure that we adopt here, which is detailed in an earlier publication [8], gives only the minima. The lowest minimum corresponds to the thermodynamically stable state, which is the one appearing in an equilibrium phase diagram. Other minima correspond to metastable states, such as the ones discussed in section 1 (e.g., the supersaturated gas) and via which transitions to the stable state occur through nucleation. It is the analysis of the metastable states that is the central concern of this article.

3. Theory

3.1. Stability limits

In order to investigate the stability of a given minimum $\boldsymbol{\rho}^0$ in the grand potential functional, we examine the 'cost' in free energy of small displacements in density $\delta\rho_i=\rho_i-\rho_i^0$ about $\boldsymbol{\rho}^0$. To this end we expand $\Omega[\boldsymbol{\rho}]$ in a Taylor series about $\boldsymbol{\rho}^0$:

$$\Omega[\boldsymbol{\rho}]\simeq\Omega[\boldsymbol{\rho}^0]+\sum_{i=1}^{\mathcal{N}}\left(\frac{\partial\Omega}{\partial\rho_i}\right)_0(\rho_i-\rho_i^0)+\frac{1}{2}\sum_{i=1}^{\mathcal{N}}\sum_{j=1}^{\mathcal{N}}\left(\frac{\partial^2\Omega}{\partial\rho_i\,\partial\rho_j}\right)_0(\rho_i-\rho_i^0)(\rho_j-\rho_j^0)+\cdots \tag{3.1}$$

ignoring contributions of degree higher than the second. Since $\Omega[\boldsymbol{\rho}^0]$ is a minimum, $(\partial\Omega/\partial\rho_i)_0$ vanishes. Thus, (3.1) can be recast compactly as

$$\delta\Omega[\delta\boldsymbol{\rho}]\equiv\Omega[\boldsymbol{\rho}]-\Omega[\boldsymbol{\rho}^0]=\tfrac{1}{2}\,\delta\boldsymbol{\rho}^{\rm T}\cdot\mathbf{H}\cdot\delta\boldsymbol{\rho} \tag{3.2}$$

where $\mathbf{H}$ is the $(\mathcal{N}\times\mathcal{N})$ Hessian matrix with elements $H_{ij}=(\partial^2\Omega/\partial\rho_i\,\partial\rho_j)_0$; $\delta\boldsymbol{\rho}$ is the $\mathcal{N}$-dimensional column vector whose elements are $\delta\rho_i=\rho_i-\rho_i^0$ and $\delta\boldsymbol{\rho}^{\rm T}$ is its transpose. From (2.6) and (2.7) we deduce

$$H_{ij}=\left(\frac{\partial^2\mathcal{F}_{\rm id}}{\partial\rho_i\,\partial\rho_j}\right)_0+\left(\frac{\partial^2\mathcal{F}_{\rm ex}}{\partial\rho_i\,\partial\rho_j}\right)_0=\frac{\beta^{-1}\delta_{ij}}{\rho_i^0(1-\rho_i^0)}+u_{\rm a}(i,j) \tag{3.3}$$

where δ_{ij} is the Kronecker symbol.

Because $u_{\rm a}(i,j)$ depends only on the distance vector between sites i and j, $u_{\rm a}(i,j)=u_{\rm a}(j,i)$. Since ρ_i^0 and $u_{\rm a}$ are also real, it follows from (3.3) that $H_{ij}=H_{ji}=H_{ji}^*$, where the asterisk stands for the complex conjugate. Therefore, $\mathbf{H}$ is Hermitian and consequently can be diagonalized by a unitary transformation. That is,

$$\mathbf{U}^{\rm T}\cdot\mathbf{H}\cdot\mathbf{U}=\boldsymbol{\Lambda} \tag{3.4}$$

where $\boldsymbol{\Lambda}$ is a diagonal matrix with elements λ_l $(l=1,2,\ldots,\mathcal{N})$. Defining the column vector of the normal displacement modes by

$$\delta\boldsymbol{Q}=\mathbf{U}^{\rm T}\cdot\delta\boldsymbol{\rho} \tag{3.5}$$

we can rewrite (3.2) as

$$\delta\Omega=\tfrac{1}{2}\delta\boldsymbol{Q}^{\rm T}\cdot\boldsymbol{\Lambda}\cdot\delta\boldsymbol{Q}=\tfrac{1}{2}\sum_{l=1}^{\mathcal{N}}\lambda_l\,\delta q_l^2 \tag{3.6}$$

where q_l is the lth normal mode given in terms of the original displacements by

$$\delta q_l = \sum_{j=1}^{\mathcal{N}} u_{jl}\, \delta\rho_j. \tag{3.7}$$

In (3.7), u_{jl} is the jth component of the eigenvector $\boldsymbol{u}_l$ of $\mathbf{H}$, which is the lth column vector of $\mathbf{U}$ and the eigenvalue λ_l is the effective 'force constant' associated with the mode.

Since the λs depend on $\boldsymbol{\rho}^0$, they are implicit functions of the thermodynamic state variables μ and T and also of the model parameters (i.e., n_z, ϵ_{fw}, ϵ_{ff}). As long as $\boldsymbol{\rho}^0$ minimizes $\Omega[\boldsymbol{\rho}]$, all λs are positive and any displacement $\delta\boldsymbol{\rho}$ is countered by a 'restoring force'. Note that this latter statement holds for both *local* minima and for the *global* minimum. In other words, knowledge of the λs alone is insufficient to indicate whether the state corresponding to $\boldsymbol{\rho}^0$ is (globally) stable, or merely metastable. As the state approaches a spinodal, however, a certain 'dominant' eigenvalue, say λ_{d}, begins to decrease markedly, indicating that displacements in the dominant normal mode are opposed by a sharply reduced restoring force. As the spinodal is reached, λ_{d} vanishes; the minimum turns into a saddle point and the restoring force vanishes. The metastable state has reached its limit of stability.

Although the above analysis provides well-defined criteria for stability, it does not address the physical interpretation of the dominant or 'soft' modes. From a mathematical viewpoint, the dominant mode indicates the directions in $\boldsymbol{\rho}$-space in which $\Omega[\boldsymbol{\rho}]$ flattens most rapidly as the spinodal is approached. One might therefore expect the dominant mode to give some indication of the morphology of the phase beyond the spinodal. Indeed similar stability analyses within the context of homogeneous binary fluids [22, 23] and polar fluids [24] have shown that the dominant mode can be a reliable indicator of the nature of the 'new' phase. This experience also suggests a further interpretation of the dominant mode, namely that its direction in $\boldsymbol{\rho}$-space may indicate the pathway from the metastable to the new stable phase.

In general, however, one appears to face the discouraging prospect of having to examine the dependence of all $\mathcal{N}$ eigenvalues of $\mathbf{H}$ on the thermodynamic state. However, if the system possesses symmetries beyond those implied in the general description of the model given in section 2, then it is possible to exploit these symmetries by expressing the Hessian in an alternative (reciprocal-space) representation where it becomes block-diagonal. In the next section we demonstrate how to carry out this simplification for the special case of a slit-pore with chemically homogeneous walls.

3.2. The slit-pore with homogeneous walls

In the case where the walls are smooth on an infinitesimal scale, Φ_i depends only on the distance of site i from either wall. Then, for the solutions $\boldsymbol{\rho}^0$ of (2.10) that minimize $\Omega[\boldsymbol{\rho}]$, $\boldsymbol{\rho}^0$ is constant in planes parallel with the walls. That is, the densities ρ_i^0 on all M^2 lattice sites in a given plane $z = m_z$ ($m_z = 1, 2, \ldots, n_z$) are equal. Thus, equation (2.10) involves only n_z *a priori* unknown densities. If the lattice sites are labelled explicitly by the dual index $i \equiv (\boldsymbol{R}, m_z)$, where the two-dimensional vector $\boldsymbol{R} \equiv (m_x, m_y)$, then (3.2) becomes

$$\delta\Omega = \tfrac{1}{2} \sum_{\boldsymbol{R}} \sum_{m_z} \sum_{\boldsymbol{R}'} \sum_{m_z'} \delta\rho(\boldsymbol{R}, m_z)\, H(\boldsymbol{R}, m_z; \boldsymbol{R}', m_z')\, \delta\rho(\boldsymbol{R}', m_z') \tag{3.8}$$

where the subscripts are now indicated in parentheses to ease the notational burden. Because of the in-plane symmetry pointed out above, every lattice site in a given plane $z = m_z$ is equivalent. The Hessian matrix elements therefore depend only on the *vector difference* $\boldsymbol{R} - \boldsymbol{R}'$ rather than on both $\boldsymbol{R}$ and $\boldsymbol{R}'$ separately. This can be seen more clearly by recasting H_{ij} given in (3.3) in

the dual-index notation as

$$H(\boldsymbol{R}, m_z; \boldsymbol{R}', m_z') = \frac{\beta^{-1}\delta_{\boldsymbol{R},\boldsymbol{R}'}\delta_{m_z,m_z'}}{\rho^0_{m_z}(1-\rho^0_{m_z})} + u_{\mathrm{a}}(\boldsymbol{R}-\boldsymbol{R}', m_z - m_z') \tag{3.9}$$

where we have used that the pair potential depends only on the distance *vector* between sites $i = (\boldsymbol{R}, m_z)$ and $j = (\boldsymbol{R}', m_z')$. We can exploit the equivalence of sites within a given plane to reduce drastically the effort of finding the normal displacement modes. This simplification is effected by introducing the discrete Fourier transform (see appendix A).

We can therefore represent the Hessian in terms of the two-dimensional basis vectors (see (A.6)) as

$$H(\boldsymbol{R}, m_z; \boldsymbol{R}', m_z') = \sum_{\boldsymbol{k}} \tilde{H}(\boldsymbol{k}, m_z, m_z')\Psi_{\boldsymbol{k}}(\boldsymbol{R}-\boldsymbol{R}'). \tag{3.10}$$

Likewise we can express the displacements of the local density as

$$\delta\rho(\boldsymbol{R}, m_z) = \sum_{\boldsymbol{k}'} \delta\tilde{\rho}(\boldsymbol{k}', m_z)\, \Psi_{\boldsymbol{k}'}(\boldsymbol{R}). \tag{3.11}$$

Note that $\tilde{H}$ and $\delta\tilde{\rho}$ stand for 'partial' transforms, still depending on the indices m_z and m_z' of the two lattice planes involved. After substituting into (3.8) the expressions given in (3.10) and (3.11), and simplifying the result, we arrive at

$$\delta\Omega = \tfrac{1}{2}\sum_{\boldsymbol{k}}\sum_{m_z}\sum_{m_z'} \delta\tilde{\rho}^*(\boldsymbol{k}, m_z)\, M\tilde{H}(\boldsymbol{k}, m_z, m_z')\, \delta\tilde{\rho}(\boldsymbol{k}, m_z'). \tag{3.12}$$

From (3.9) we obtain for the Hessian in reciprocal space

$$M\tilde{H}(\boldsymbol{k}, m_z, m_z') = \frac{\beta^{-1}\delta_{m_z,m_z'}}{\rho^0_{m_z}(1-\rho^0_{m_z})} + M\tilde{u}_{\mathrm{a}}(\boldsymbol{k}, m_z - m_z') \tag{3.13}$$

using the relation given in (A.9). The Fourier component of the pair potential $\tilde{u}_{\mathrm{a}}$ is specified in section 3.3.

We now observe that since different reciprocal vectors $\boldsymbol{k}$ are not coupled in $\delta\Omega$, we can recast (3.12) as

$$\delta\Omega = \sum_{\boldsymbol{k}} \delta\Omega_{\boldsymbol{k}} \tag{3.14}$$

where

$$\delta\Omega_{\boldsymbol{k}} = \tfrac{1}{2}\delta\tilde{\boldsymbol{\rho}}^{\dagger}(\boldsymbol{k}) \cdot M\tilde{\mathbf{H}}(\boldsymbol{k}) \cdot \delta\tilde{\boldsymbol{\rho}}(\boldsymbol{k}). \tag{3.15}$$

In (3.15) we used the compact notation introduced in section 3.1, the dagger denotes the Hermitian adjoint, and the elements of $\tilde{\mathbf{H}}(\boldsymbol{k})$ are $\tilde{H}(\boldsymbol{k}, m_z, m_z')$ (see (3.13)). The sum on $\boldsymbol{k}$ in (3.14) runs over the M^2 blocks, where the contribution of each block is given by (3.15). In other words, in reciprocal space the original $M^2 n_z \times M^2 n_z$ Hessian $H(\boldsymbol{R}, m_z; \boldsymbol{R}', m_z')$ reduces to block-diagonal form, where the M^2 blocks are labelled by $\boldsymbol{k}$ and each block has dimensions $n_z \times n_z$. Because the lattice is centrosymmetric it follows that $\tilde{\mathbf{H}}$ is real and symmetric and can therefore be brought to diagonal form by a unitary transformation in the same fashion as detailed in section 3.1. The result is

$$\delta\Omega_{\boldsymbol{k}} = \tfrac{1}{2}\sum_{l=1}^{n_z} \lambda_l(\boldsymbol{k})|q_l(\boldsymbol{k})|^2 \tag{3.16}$$

where now the eigenvalues $\lambda_l(\boldsymbol{k})$ and the corresponding normal modes

$$q_l(\boldsymbol{k}) = \sum_{m_z=1}^{n_z} u_{m_z l}\, \delta\tilde{\rho}(\boldsymbol{k}, m_z) \tag{3.17}$$

depend on $\boldsymbol{k}$ as well as on the thermodynamic state variables and model parameters implicitly. Note that because of the argument presented in section 3.1, the state corresponding to $\{\rho^0_{m_z}, m_z = 1, 2, \ldots, n_z\}$ is thermodynamically stable or metastable as long as $\lambda_l(\boldsymbol{k}) > 0$ for all l and $\boldsymbol{k}$.

3.3. Nearest-neighbour interactions

In the special case of principal concern to us, where only nearest-neighbour interactions are taken into account, the pair potential in real space takes the form

$$u_{\mathrm{a}}(\boldsymbol{R} - \boldsymbol{R}', m_z - m_z') = -\epsilon_{\mathrm{ff}}[\delta_{m_z,m_z'}\delta_{\boldsymbol{R}-\boldsymbol{R}',\boldsymbol{d}_\parallel} + \delta_{\boldsymbol{R},\boldsymbol{R}'}(\delta_{m_z-m_z',1} + \delta_{m_z-m_z',-1})] \tag{3.18}$$

where $-\epsilon_{\mathrm{ff}}$ is the potential energy of attraction between neighbouring molecules and $\boldsymbol{d}_\parallel$ is a vector from reference site $\boldsymbol{R}$ to one of its nearest neighbours in the x–y plane. Using (A.6), (A.9), and (A.10) we obtain for the pair potential in reciprocal space

$$M\tilde{u}_{\mathrm{a}}(\boldsymbol{k}, m_z, m_z') = -\epsilon_{\mathrm{ff}}\left[\delta_{m_z,m_z'}\sum_{\boldsymbol{d}_\parallel}\exp\left(-\frac{2\pi \mathrm{i}\boldsymbol{k}\cdot\boldsymbol{d}_\parallel}{M}\right) + \delta_{m_z-m_z',1} + \delta_{m_z-m_z',-1}\right]. \tag{3.19}$$

The sum in (3.19) is over the unit vectors $(\hat{\boldsymbol{e}}_x, 0)$, $(\hat{\boldsymbol{e}}_y, 0)$, $(-\hat{\boldsymbol{e}}_x, 0)$, $(-\hat{\boldsymbol{e}}_y, 0)$. Combining (3.13) and (3.19), we arrive at the following explicit form for the reciprocal-space Hessian:

$$\begin{aligned} M\tilde{H}(\boldsymbol{k}, m_z, m_z') = {} & \frac{\beta^{-1}\delta_{m_z,m_z'}}{\rho^0_{m_z}(1-\rho^0_{m_z})} - 2\epsilon_{\mathrm{ff}}\left[\cos\left(\frac{2\pi k_x}{M}\right) + \cos\left(\frac{2\pi k_y}{M}\right)\right]\delta_{m_z,m_z'} \\ & - \epsilon_{\mathrm{ff}}[\delta_{m_z,m_z'-1} + \delta_{m_z,m_z'+1}]. \end{aligned} \tag{3.20}$$

Noting that the $\boldsymbol{k}$-dependence of $M\tilde{\mathbf{H}}$ appears only on the diagonal and that the dependence is identical for all elements, we can rewrite (3.20) as

$$M\tilde{\mathbf{H}} = M\tilde{\mathbf{H}}' + \Phi(\boldsymbol{k})\mathbf{1} \tag{3.21}$$

where $\mathbf{1}$ is the identity matrix, the elements of $M\tilde{\mathbf{H}}'$:

$$M\tilde{H}'(m_z, m_z') \equiv \frac{\beta^{-1}\delta_{m_z,m_z'}}{\rho^0_{m_z}(1-\rho^0_{m_z})} - \epsilon_{\mathrm{ff}}[\delta_{m_z,m_z'-1} + \delta_{m_z,m_z'+1}] \tag{3.22}$$

are independent of $\boldsymbol{k}$, and the *scalar* function $\Phi(\boldsymbol{k})$ is defined by

$$\Phi(\boldsymbol{k}) \equiv -2\epsilon_{\mathrm{ff}}\left[\cos\left(\frac{2\pi k_x}{M}\right) + \cos\left(\frac{2\pi k_y}{M}\right)\right]. \tag{3.23}$$

It follows immediately from (3.21) that $M\tilde{\mathbf{H}}$ is diagonalized by the same unitary transformation as diagonalizes $M\tilde{\mathbf{H}}'$. In other words, the two matrices have the same eigenvectors. Furthermore, the eigenvalues of $M\tilde{\mathbf{H}}$ are given by

$$\lambda_l(\boldsymbol{k}) = \lambda_l' + \Phi(\boldsymbol{k}) \tag{3.24}$$

where λ_l' is the lth eigenvalue of $M\tilde{\mathbf{H}}'$.

The task of determining the eigenvalues of $M\tilde{\mathbf{H}}(\boldsymbol{k})$ therefore reduces to that of diagonalizing the single $n_z \times n_z$ tridiagonal Hermitian matrix $M\tilde{\mathbf{H}}'$. The latter does not depend on $\boldsymbol{k}$; its eigenvalues and eigenvectors are functions only of the thermodynamic state variables and the model parameters. Note also from the functional form of $\Phi(\boldsymbol{k})$ given in (3.23) that the eigenvalues of $M\tilde{\mathbf{H}}$ assume their lowest numerical values at $\boldsymbol{k} = \mathbf{0}$, regardless of l. We therefore expect the harbinger of the spinodal to be a $\boldsymbol{k} = \mathbf{0}$ normal mode and restrict our attention primarily to the long-wavelength limit henceforth.

3.4. Correlations in the local density

Added insight into mechanistic aspects of the transition may be achieved by studying the behaviour of density fluctuations as the spinodal is approached. Along the 'quasistatic trajectory' of the metastable minimum, equation (2.9) holds. That is, everywhere along the trajectory we solve (2.9) to obtain the local density $\boldsymbol{\rho}^0$ as a function of μ and T. We can also regard μ, or μ_i, as a function of $\boldsymbol{\rho}^0$ and differentiate both sides of (2.9) with respect to ρ_j^0 along the trajectory to obtain

$$-\beta\left(\frac{\partial^2\mathcal{F}_{\rm ex}}{\partial\rho_i\,\partial\rho_j}\right)_0 = \frac{\delta_{ij}}{\rho_i^0(1-\rho_i^0)} + \beta\left(\frac{\partial\mu_i}{\partial\rho_j}\right)_0 = -\beta u_{\rm a}(i,j) \tag{3.25}$$

where the far right side of (3.25) follows from (2.7). By direct differentiation of the formally exact expression for the grand potential Ω given in (2.3), we also obtain

$$\left(\frac{\partial\Omega}{\partial\mu_i}\right) = \langle s_i\rangle \tag{3.26}$$

$$\left(\frac{\partial^2\Omega}{\partial\mu_i\,\partial\mu_j}\right) = \beta[\langle s_i\rangle\langle s_j\rangle - \langle s_i s_j\rangle] \tag{3.27}$$

where the angular brackets signify the grand ensemble average.

We now define the density–density response function

$$G_{ij} \equiv -\beta^{-1}\left(\frac{\partial^2\Omega}{\partial\mu_i\,\partial\mu_j}\right)_0 = \langle s_i s_j\rangle - \langle s_i\rangle\langle s_j\rangle = \langle\delta s_i\,\delta s_j\rangle = -\beta^{-1}\left(\frac{\partial\rho_i}{\partial\mu_j}\right)_0 \tag{3.28}$$

where $\delta s_i \equiv s_i - \langle s_i\rangle$ and the right-hand side follows from (3.27). To arrive at the third member of the equality we have set $\langle s_i\rangle = \rho_i^0$ in (3.26). Now substituting expressions for $(\partial\mu_i/\partial\rho_k)_0$ and $(\partial\rho_k/\partial\mu_j)_0$, respectively given in (3.25) and (3.28), into the identity

$$\sum_k\left(\frac{\partial\mu_i}{\partial\rho_k}\right)_0\left(\frac{\partial\rho_k}{\partial\mu_j}\right)_0 = \delta_{ij} \tag{3.29}$$

we obtain

$$\beta\mathbf{H}\cdot\mathbf{G} = \mathbf{1} \tag{3.30}$$

where $\mathbf{H}$ is the real-space Hessian and $\mathbf{G}$ is the matrix of density–density correlation functions. Equation (3.30) is the lattice-gas analogue of the Ornstein–Zernike equation of liquid-state theory [25,26], which provides, in principle, an exact relation between density correlations and the Hessian. In particular, the interaction contribution to $\mathbf{H}$ (i.e., $(\partial^2\mathcal{F}_{\rm ex}/\partial\rho_i\,\partial\rho_j)_0$, see (3.25)) is just the so-called 'direct correlation function', which, in the mean-field approximation, reduces to the intermolecular potential.

In section 3.2 we demonstrated explicitly that on account of the symmetry of the slit-pore with homogeneous walls the $(\boldsymbol{R}, m_z; \boldsymbol{R}', m_z')$ element of $\mathbf{H}$ depends on $\boldsymbol{R}$ and $\boldsymbol{R}'$ only through the difference vector $\boldsymbol{R}-\boldsymbol{R}'$. The same argument applies to the elements of $\mathbf{G}$. Therefore, we can write the following expression for $\mathbf{G}$ in analogy to (3.10):

$$G(\boldsymbol{R}'', m_z''; \boldsymbol{R}', m_z') = \sum_{\boldsymbol{k}'}\tilde{G}(\boldsymbol{k}', m_z'', m_z')\Psi_{\boldsymbol{k}'}(\boldsymbol{R}''-\boldsymbol{R}'). \tag{3.31}$$

Substituting into (3.30) the expressions for $\mathbf{G}$ and $\mathbf{H}$ respectively given in (3.31) and (3.10), we obtain

$$\sum_{\boldsymbol{k}}\left\{\sum_{m_z''}M\tilde{H}(\boldsymbol{k}, m_z, m_z'')M\tilde{G}(\boldsymbol{k}, m_z'', m_z') - \beta^{-1}\delta_{m_z m_z'}\right\}\Psi_{\boldsymbol{k}}(\boldsymbol{R}-\boldsymbol{R}') = 0 \tag{3.32}$$

which follows from the definition of $\Psi_k(\boldsymbol{R})$ given in (A.1). We then conclude on the basis of the orthogonality relations (A.2) and (A.3) that the coefficient of $\Psi_k(\boldsymbol{R}-\boldsymbol{R}')$ in brackets in (3.32) must vanish. We thus arrive at the reciprocal-space representation of the real-space relation (3.30):

$$M\tilde{\mathbf{H}}(\boldsymbol{k})\cdot M\tilde{\mathbf{G}}(\boldsymbol{k})=\beta^{-1}\mathbf{1} \tag{3.33}$$

in which all matrices have dimensions $n_z \times n_z$. It follows directly from (3.33) that

$$\tilde{\mathbf{G}}(\boldsymbol{k})=\frac{1}{\beta M}[M\tilde{\mathbf{H}}(\boldsymbol{k})]^{-1}. \tag{3.34}$$

Moreover, it follows from (3.34) that $\tilde{\mathbf{G}}$ is diagonalized by the same unitary transformation as diagonalizes $M\tilde{\mathbf{H}}$. To demonstrate this we perform the same unitary transformation on (3.34) as diagonalizes $\tilde{\mathbf{H}}$. The result is

$$\mathbf{E}=\mathbf{U}^{\mathrm{T}}\cdot\tilde{\mathbf{G}}(\boldsymbol{k})\cdot\mathbf{U}=\beta^{-1}M^{-1}\mathbf{\Lambda}^{-1} \tag{3.35}$$

where $\mathbf{\Lambda}$ is the *diagonal* matrix containing the eigenvalues of $M\tilde{\mathbf{H}}$. Equation (3.35) implies that $\mathbf{E}$ is diagonal as well. The diagonal elements of $\mathbf{E}$ and $\mathbf{\Lambda}$ are therefore related by

$$\eta_l(\boldsymbol{k})=\frac{1}{\beta M\lambda_l(\boldsymbol{k})} \qquad l=1,2,\ldots,n_z \tag{3.36}$$

where $\lambda_l(\boldsymbol{k})$ is the eigenvalue of $M\tilde{\mathbf{H}}$ associated with the lth normal displacement mode. Moreover, it follows from (3.35) that the eigenvalues of $\tilde{\mathbf{G}}$ can be expressed as

$$\eta_l(\boldsymbol{k})=(\mathbf{E})_{ll}=(\mathbf{U}^{\mathrm{T}}\cdot\tilde{\mathbf{G}}\cdot\mathbf{U})_{ll}=\sum_{m_z}\sum_{m_z'}u_{m_z l}u_{m_z' l}\tilde{G}(\boldsymbol{k},m_z,m_z') \tag{3.37}$$

where the $u_{m_z l}$ are components of the eigenvectors $\boldsymbol{u}_l$ of $M\tilde{\mathbf{H}}$. From (3.37) it is clear that since adjacent planes are coupled in $M\tilde{\mathbf{H}}$, the eigenvalues $\eta_l(\boldsymbol{k})$ of $\tilde{\mathbf{G}}$ are not, as would appear to be the case, true in-plane (2D) correlation functions. Rather they describe the mean squared density fluctuations both within and 'between' planes of the lattice. The contributions of the various layers to $\eta_l(\boldsymbol{k})$ are given by the eigenvectors of $M\tilde{\mathbf{H}}$, which are also eigenvectors of $\tilde{\mathbf{G}}$.

We now envisage the system approaching an instability (i.e., some eigenvalue of the Hessian is going to zero). From (3.36) it is immediately clear that the vanishing force constant implies a *divergence* of the related mean squared density fluctuations in reciprocal space. Furthermore, we already know that only the $\boldsymbol{k}=\mathbf{0}$ mode can become dominant (see the discussion below (3.24)). Therefore, the divergence of the fluctuations also occurs at $\boldsymbol{k}=\mathbf{0}$. This implies that the density correlations in *real* space (i.e., the functions $G(\boldsymbol{R},m_z;\boldsymbol{R}',m_z')$ which are the inverse Fourier transforms of $\tilde{G}(\boldsymbol{k},m_z,m_z')$) are becoming long range; that is, the so-called correlation length is diverging. In the following we wish to describe this phenomenon more explicitly by relating the long-range behaviour (i.e., the asymptotic behaviour as $R\to\infty$) of the real-space density correlations $G(\boldsymbol{R},m_z;\boldsymbol{R}',m_z')$ to the eigenvalues λ_l at $\boldsymbol{k}=\mathbf{0}$. Our approach essentially follows the common Ornstein–Zernike theory of dominant fluctuations, as described in many textbooks in the context of liquid-state theory [27, 28]. The present case is more complicated than the one usually considered, namely *true* two- or three-dimensional systems, where only *one* length scale is involved. The reason is that our system consists of several layers, and the fluctuations in and between the layers are coupled. Therefore, the long-range behaviour of the functions $G(\boldsymbol{R},m_z;\boldsymbol{R}',m_z')$ is coupled as well.

We start by expressing the $\tilde{G}(\boldsymbol{k},m_z,m_z')$ (i.e., the Fourier transform of the quantities that we are interested in) in terms of $\eta_l(\boldsymbol{k})$, which are just the inverse eigenvalues $\lambda_l(\boldsymbol{k})$. Using (3.35) and (3.36) we find

$$\tilde{G}(\boldsymbol{k},m_z,m_z')=(\mathbf{U}\cdot\mathbf{E}\cdot\mathbf{U}^{\mathrm{T}})_{m_z,m_z'}=\sum_{l=1}^{n_z}u_{m_z l}u_{m_z' l}\eta_l(\boldsymbol{k}). \tag{3.38}$$

We now make use of the fact that, within the present approximations, the components $u_{m_z l}$ of the eigenvectors do *not* themselves depend on $\boldsymbol{k}$. As a result, the Fourier back-transform of $\tilde{\mathbf{G}}(\boldsymbol{k}, m_z, m_z')$ can be written simply as

$$G(\boldsymbol{R}, m_z; \boldsymbol{R}', m_z') = \sum_{\boldsymbol{k}} \tilde{G}(\boldsymbol{k}, m_z, m_z')\Psi_{\boldsymbol{k}}(\boldsymbol{R} - \boldsymbol{R}') = \sum_{l=1}^{n_z} u_{m_z l} u_{m_z' l} \eta_l(\boldsymbol{R} - \boldsymbol{R}') \tag{3.39}$$

where the far right side follows from (3.38) and

$$\eta_l(\boldsymbol{R} - \boldsymbol{R}') = \sum_{\boldsymbol{k}} \eta_l(\boldsymbol{k})\Psi_{\boldsymbol{k}}(\boldsymbol{R} - \boldsymbol{R}'). \tag{3.40}$$

Equation (3.39) implies that the asymptotic behaviour of $G(\boldsymbol{R}, m_z; \boldsymbol{R}', m_z')$ is determined only by that of the functions $\eta_l(\boldsymbol{R} - \boldsymbol{R}')$ which can be computed from (3.40) combined with (3.36).

To evaluate the inverse transform (3.40), we first note that, because of the functional form of $\Psi_{\boldsymbol{k}}(\boldsymbol{R})$ (see (A.1)), the summation over the indices k_x and k_y can be replaced by a summation over transformed indices $\kappa_x \equiv 2\pi k_x/M$ and $\kappa_y \equiv 2\pi k_y/M$. Equation (3.40) then becomes

$$\eta_l(\boldsymbol{R}) = \frac{1}{M} \sum_{\boldsymbol{\kappa}} \eta_l(\boldsymbol{\kappa}) \exp(\mathrm{i}\boldsymbol{\kappa} \cdot \boldsymbol{R}) \tag{3.41}$$

where $\boldsymbol{\kappa} = (\kappa_x, \kappa_y)$. (In (3.41) we have temporarily set $\boldsymbol{R} - \boldsymbol{R}'$ equal to $\boldsymbol{R}$ to simplify the notation.) In the limit of an infinite system ($M \to \infty$) the distance $\Delta\kappa = 2\pi/M$ between neighbouring points in reciprocal space becomes infinitesimally small. Therefore, the double sum in (3.41) can be replaced by the double integral

$$\begin{aligned} \eta_l(\boldsymbol{R}) &= \frac{1}{M(\Delta\kappa)^2} \int_{-\pi}^{\pi} \mathrm{d}\kappa_x \int_{-\pi}^{\pi} \mathrm{d}\kappa_y \, \eta_l(\boldsymbol{\kappa}) \exp(\mathrm{i}\boldsymbol{\kappa} \cdot \boldsymbol{R}) \\ &= \frac{1}{\beta(2\pi)^2} \int_{-\pi}^{\pi} \mathrm{d}\kappa_x \int_{-\pi}^{\pi} \mathrm{d}\kappa_y \, \lambda_l^{-1}(\boldsymbol{\kappa}) \exp(\mathrm{i}\boldsymbol{\kappa} \cdot \boldsymbol{R}) \end{aligned} \tag{3.42}$$

where we have used (3.36) to obtain the last line.

We now expand $\lambda_l(\boldsymbol{\kappa})$ around $\boldsymbol{\kappa} = \mathbf{0}$. This is justified as long as we are interested only in the long-range behaviour of $\eta_l(\boldsymbol{R})$. From (3.23) and (3.24) we obtain

$$\lambda_l(\boldsymbol{\kappa}) \simeq \lambda_l' - 4\epsilon_{\mathrm{ff}} + \boldsymbol{\kappa} \cdot \boldsymbol{\kappa} + \mathrm{O}(\kappa^4) \simeq \lambda_l(0) + \kappa^2 \tag{3.43}$$

where $\lambda_l(0) \equiv \lambda_l(\boldsymbol{\kappa} = \mathbf{0})$. We note in passing that, as a result of the mean-field approximation, the prefactor of κ^2 (1) in (3.43) is independent of the thermodynamic state. Furthermore, since the expanded $\lambda_l(\boldsymbol{\kappa})$ involves only the magnitude of $\boldsymbol{\kappa}$, the real-space correlation η_l depends only on $R = |\boldsymbol{R}|$. Substituting this expression for $\lambda_l(\boldsymbol{\kappa})$ in (3.42) and transforming to polar coordinates, we obtain

$$\eta_l(R) \simeq \frac{1}{4\pi^2\beta} \int_0^{2\pi} \mathrm{d}\varphi \int_0^{\kappa(\varphi)} \mathrm{d}\kappa \, \frac{\kappa \exp(\mathrm{i}\kappa R \cos\varphi)}{\lambda_l(0) + \kappa^2} \tag{3.44}$$

where the dependence of the upper limit of the κ-integration on φ results from the square boundary in the original Cartesian space (see (3.42)). This integral has already been dealt with in the context of the critical behaviour of *truly* two-dimensional systems [28, 29].

Assuming that $\lambda_l(0)$ is positive we find (see appendix B) in the asymptotic (large-R) limit

$$\eta_l(R) \simeq \frac{1}{2\beta\sqrt{2\pi}} \sqrt{\frac{\xi_l}{R}} \exp(-R/\xi_l) \qquad R \to \infty \tag{3.45}$$

where the 'correlation length' $\xi_l \equiv 1/\sqrt{\lambda_l(0)}$. Equation (3.45) shows that correlations $\eta_l(R)$ decay exponentially and that the correlation length diverges as $\lambda_l(0) \to 0$. Note, however,

that (3.45) is strictly valid only for $\lambda_l(0) > 0$. Directly at $\lambda_l(0) = 0$, the integral in (3.44) results in (unphysical) logarithmic behaviour of $\eta_l(R)$ [29].

Finally, combining (3.45) and (3.39), we find that the asymptotic behaviour of the correlation functions $G(\boldsymbol{R}, m_z; \boldsymbol{R}', m_z')$ is given as a *sum* of exponentials:

$$G(\boldsymbol{R}, m_z; \boldsymbol{R}', m_z') \simeq \sum_{l=1}^{n_z} u_{m_z l} u_{m_z' l} \frac{1}{2\beta\sqrt{2\pi}} \sqrt{\frac{\xi_l}{|\boldsymbol{R} - \boldsymbol{R}'|}} \exp(-|\boldsymbol{R} - \boldsymbol{R}'|/\xi_l). \tag{3.46}$$

This shows that even an in-plane correlation function $G(\boldsymbol{R}, m_z; \boldsymbol{R}', m_z' = m_z)$ is governed by several correlation lengths.

4. Results

4.1. State-independent properties of displacement modes

As an illustration of the application of the formalism developed in section 3 we consider the special case of the slit-pore with homogeneous walls. We invoke the nearest-neighbour approximation and take the 'external' field due to the walls to act only on fluid molecules in the 'contact' layers:

$$\Phi_i = -\epsilon_{\mathrm{fw}}(\delta_{m_z,1} + \delta_{m_z,n_z}) \tag{4.1}$$

where ϵ_{fw} is the depth of the fluid–wall attraction. Henceforth we adopt the customary dimensionless units: distance in units of the lattice constant σ, energy in units of ϵ_{ff}, and temperature in units of $\epsilon_{\mathrm{ff}}/k_{\mathrm{B}}$. The thermodynamic state is then specified by independent state variables μ, T, n_z, and ϵ_{fw}.

On account of the mirror symmetry about the mid-plane, the number of *a priori* unknown densities $\{\rho_i^0\}$ which satisfy (2.10) is $n_z/2$ if n_z is even, or $(n_z + 1)/2$ if n_z is odd. We now specialize our considerations even further to the simple, yet nevertheless nontrivial, case $n_z = 3$, which involves only the two *a priori* unknown densities $\rho_1^0 = \rho_3^0$ and ρ_2^0. These must satisfy (2.10), which can be written as

$$T \ln\left(\frac{\rho_1^0}{1-\rho_1^0}\right) - 4\rho_1^0 - \rho_2^0 + \mu_1 = 0 \qquad T \ln\left(\frac{\rho_2^0}{1-\rho_2^0}\right) - 4\rho_2^0 - 2\rho_1^0 + \mu_2 = 0. \tag{4.2}$$

In (4.2), $\mu_1 = -\epsilon_{\mathrm{fw}} - \mu$, $\mu_2 = -\mu$, and we have already imposed the requirement of mirror symmetry.

In reciprocal space the $\boldsymbol{k}$-independent part of the Hessian for $n_z = 3$ assumes the form (see (3.21) (3.22))

$$M\tilde{\mathbf{H}}' = M\tilde{\mathbf{H}} - \Phi(\boldsymbol{k})\mathbf{1} = \begin{pmatrix} \alpha & -1 & 0 \\ -1 & \beta & -1 \\ 0 & -1 & \alpha \end{pmatrix} \tag{4.3}$$

where $\Phi(\boldsymbol{k})$ is given by (3.23) and

$$\alpha \equiv \frac{T}{\rho_1^0(1-\rho_1^0)} \qquad \beta \equiv \frac{T}{\rho_2^0(1-\rho_2^0)}. \tag{4.4}$$

The eigenvalues λ_l' and eigenvectors $\boldsymbol{u}_l$ of $M\tilde{\mathbf{H}}'$ can be obtained in closed form and are listed in table 1. The eigenvalues of the complete Hessian $M\tilde{\mathbf{H}}$ are then given in terms of λ_l' by (3.24). The eigenvectors of $M\tilde{\mathbf{H}}$ coincide with those of $M\tilde{\mathbf{H}}'$.

Scrutiny of table 1 reveals that the eigenvalues λ_l' are ordered independently of the thermodynamic state and of the parameter ϵ_{fw}. To see this we first note that, according to

Table 1. Eigenvalues and components u_{l,m_z} of the (unnormalized) eigenvectors of the matrix $M\tilde{\mathbf{H}}'$ for $n_z = 3$; $\alpha = T/\rho_1^0(1-\rho_1^0)$, $\beta = T/\rho_2^0(1-\rho_2^0)$.

l	λ_l'	$(u_{1l}; u_{2l}; u_{3l})$
1	$\frac{1}{2}\{(\alpha+\beta) - [(\alpha-\beta)^2+8]^{1/2}\}$	$(1, \frac{1}{2}\{(\alpha-\beta) + [(\alpha-\beta)^2+8]^{1/2}\}, 1)$
2	α	$(1, 0, -1)$
3	$\frac{1}{2}\{(\alpha+\beta) + [(\alpha-\beta)^2+8]^{1/2}\}$	$(1, \frac{1}{2}\{(\alpha-\beta) - [(\alpha-\beta)^2+8]^{1/2}\}, 1)$

their definitions given in (4.4), α and β are positive and finite quantities, since $0 < \rho_i^0 < 1$ for $T > 0$. Furthermore, $[(\alpha-\beta)^2+8]^{1/2} > |\alpha-\beta|$, which implies the inequalities

$$\lambda_1' < \tfrac{1}{2}[(\alpha+\beta) - |\alpha-\beta|] \qquad \lambda_3' > \tfrac{1}{2}[(\alpha+\beta) + |\alpha-\beta|]. \tag{4.5}$$

If, on one hand, $\beta \leqslant \alpha$, we deduce from (4.5) that $\lambda_1' < \beta$ and $\lambda_3' > \alpha$. If, on the other hand, $\beta > \alpha$, equation (4.5) implies that $\lambda_1' < \alpha$, $\lambda_3' > \beta$. Combining these results with the fact that $\lambda_2' = \alpha$ (see table 1), we arrive at the following extended inequality:

$$\lambda_1' < \lambda_2' < \lambda_3', \tag{4.6}$$

which is valid for all possible values of α and β. Moreover, using the relation (3.24) between the eigenvalues λ_l' and those of the full Hessian, $\lambda_l(\boldsymbol{k})$, we find that the latter are ordered as well:

$$\lambda_1(\boldsymbol{k}) < \lambda_2(\boldsymbol{k}) < \lambda_3(\boldsymbol{k}) \qquad \forall\, \boldsymbol{k}. \tag{4.7}$$

Relation (4.7) implies that the cost in free energy associated with the normal displacement modes increases in the order $1 \to 2 \to 3$. In other words, mode 1 is *always* the 'softest' mode.

To understand the physical significance of the three modes, we consider the components of the eigenvectors (see table 1), since the $u_{m_z l}$ represents the amplitude of displacement in local density from its equilibrium value in lattice plane m_z. Following the same reasoning as led to (4.6), we find that the mid-plane component ($m_z = 2$) of $\boldsymbol{u}_1$ is always positive, whereas that of $\boldsymbol{u}_3$ is always negative. The latter implies that in mode 3, the density displacement in the mid-plane is opposite to that in the contact planes. In other words, mode 3 is symmetric with two nodes, and according to (4.7) we conclude that a fluctuation of this type exhibits the largest restoring force. From table 1 we find that mode 2 is antisymmetric with one node—that is, density displacements in the contact planes are in opposite directions to each other—whereas that in the mid-plane vanishes. Finally, mode 1 is symmetric without any nodes. Thus, the 'softest' mode in the three-layer system (see (4.7)) is characterized by density displacements which are in the same direction in all three lattice planes. The value of component u_{21} relative to $u_{11} = u_{31} = 1$ (see table 1) then indicates the weight of the fluctuations in the mid-plane relative to those in the contact planes.

4.2. Numerical results

Employing the iterative procedure utilized in an earlier article [8], we solved (4.2) for $\epsilon_{\mathrm{fw}} = 1.9$ and $T = 0.9$. To discuss the results it seems pedagogically most sensible to begin with the sorption isotherm, which is directly measurable in parallel sorption experiments. In figure 1 the average pore density

$$\bar{\rho} = \frac{1}{n_z}\sum_{i=1}^{n_z} \rho_{m_z}^0 = \frac{2\rho_1^0 + \rho_2^0}{3} \tag{4.8}$$

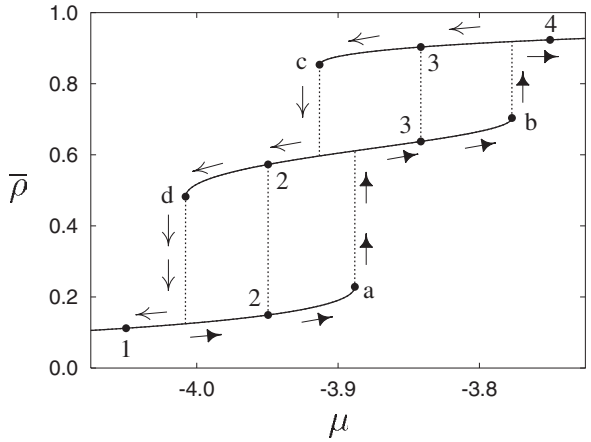

Figure 1. Average pore density $\bar{\rho}$ versus μ for $n_z = 3$, $\epsilon_{\rm fw} = 1.9$, and $T = 0.9$ for stable and metastable phases determined by solving (4.2). Labelled points are explained in the text.

is plotted as a function of μ. Three different branches between points 1 and a, d and b, and c and 4 are clearly discernible, where gas (g), monolayer (m), and liquid (l) phases may form. The gas corresponds to ρ_1^0 ($=\rho_3^0$) and ρ_2^0 both being relatively small, whereas the liquid corresponds to ρ_1^0 and ρ_2^0 being relatively large. The monolayer is characterized by relatively large ρ_1^0 but small ρ_2^0.

Suppose we perform a *gedanken* experiment in which we start from a state represented by the point 1 in figure 1 and increase μ monotonically until we reach the end point 4 on the isotherm. We then decrease μ until we arrive once again at the state point 1. The two hysteresis loops in figure 1 indicate that the 'path' traversed by the system in $\bar{\rho}$–μ space depends on the *direction* (i.e., increasing or decreasing μ) of the experiment. In order to identify stable and metastable states, we monitor the grand potential functional *density*

$$\omega[\boldsymbol{\rho}^0] = \frac{\Omega[\boldsymbol{\rho}^0]}{M^2 n_z} \tag{4.9}$$

(see (2.6)) evaluated at its minimum characterized by the density (vector) $\boldsymbol{\rho}^0$. In figure 2, $\omega[\boldsymbol{\rho}^0]$ is plotted as a function of μ for all minima, i.e. for all three phases found at $T = 0.9$. The branches and the labelled points in figure 2 correspond to those in figure 1. Note that in the presence of several minima at fixed μ (and T), the globally stable phase is that with the smallest ω; other minima correspond to metastable phases. Also, minima with the same value of ω represent coexisting phases.

At small chemical potentials, for instance at point 1 in figure 2, ω has only a single minimum at $\boldsymbol{\rho}_{\rm g}^0$ corresponding to the globally stable gas phase. When μ just barely exceeds the value associated with point d, then a second minimum at $\boldsymbol{\rho}_{\rm m}^0$ appears, which represents the monolayer phase. The minimum at $\boldsymbol{\rho}_{\rm m}^0$ is shallower than the one at $\boldsymbol{\rho}_{\rm g}^0$ and characterized by a higher value of ω; that is, $\omega[\boldsymbol{\rho}_{\rm m}^0] > \omega[\boldsymbol{\rho}_{\rm g}^0]$. Depending on the magnitude of $(\omega[\boldsymbol{\rho}_{\rm m}^0] - \omega[\boldsymbol{\rho}_{\rm g}^0])$, sooner or later a density fluctuation may arise that carries the system from the deeper to the shallower minimum, where it may reside for a while until another fluctuation brings it back to $\boldsymbol{\rho}_{\rm g}^0$. Thus, given infinite time, on average the system spends more time in the state characterized by $\boldsymbol{\rho}_{\rm g}^0$ than in the less stable one specified by $\boldsymbol{\rho}_{\rm m}^0$.

This situation changes if the chemical potential exceeds the value $\mu_x^{\rm gm} \simeq -3.95$ where $\omega[\boldsymbol{\rho}_{\rm g}^0] = \omega[\boldsymbol{\rho}_{\rm m}^0]$ (see point 2 in figures 1 and 2), and the monolayer coexists with gas. If μ

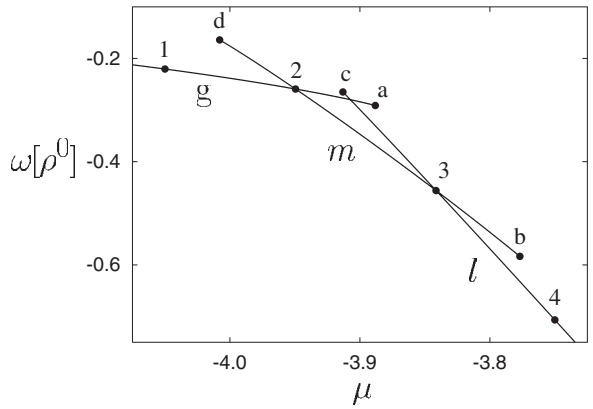

Figure 2. Grand potential density functional $\omega[\rho^0]$ versus μ for $n_z = 3$, $\epsilon_{\rm fw} = 1.9$, and $T = 0.9$ for minima determined by solving (4.2); g, m, and l correspond to gas, monolayer, and liquid morphologies described in the text; labelled points are explained in the text.

exceeds $\mu_x^{\rm gm}$ infinitesimally, the monolayer becomes globally stable. The behaviour of the experimental system now depends on the timescale allowed for equilibration. If, on the one hand, the experiment were carried out over an infinitely long time, the monolayer would eventually appear. This transformation is associated with a discontinuous change in the mean pore density indicated in figure 1 by the dotted line connecting points 2. If, on the other hand, the time allowed for equilibration is insufficient (as may be the case in typical sorption experiments), the system may persist in the (now metastable) gas phase. Only at μ corresponding to point a in figures 1 and 2 does the metastable gas phase reach its limit of stability—that is, its spinodal. In our experiment the gas phase, if it survives to point a, now spontaneously disappears to yield the monolayer corresponding to a state point in the one-phase monolayer region of the equilibrium phase diagram. The magnitude of the corresponding discontinuity in the average pore density $\bar{\rho}$ can be read off directly from the plot in figure 1.

Further information about the behaviour of the system as the spinodal is approached is displayed in figure 3. There we plot the densities in the separate planes $\rho^0_{m_z}$, the eigenvalues of $M\tilde{\mathbf{H}}(\boldsymbol{k})$ at $\boldsymbol{k} = \mathbf{0}$, and the mid-plane component u_{21} of the 'softest' normal mode, $\boldsymbol{u}_1$, over the whole range of existence of the gas phase (i.e. the branch between points 1 and a). On the scale of the plot in figure 3, $\lambda_1(0)$ and $\lambda_2(0)$ appear to coincide, but the inset shows that $\lambda_1(0) < \lambda_2(0)$, in agreement with (4.7). Moreover, only $\lambda_1(0)$ goes to zero as the spinodal is reached. Note that $u_{21} \ll 1$, which indicates that the major displacements in the softest mode occur in the 'contact' planes ($m_z = 1, 3$). This is consistent with the plot of the $\rho^0_{m_z}$, which shows that the discontinuity in local density at the spinodal is much greater in the contact planes than in the mid-plane ($m_z = 2$).

Now as μ continues to increase from point a, the system remains in the monolayer phase at least to point 3. Here, $\omega[\boldsymbol{\rho}^0_{\rm m}] = \omega[\boldsymbol{\rho}^0_{\rm l}]$ (see figure 2), which implies that for μ infinitesimally larger than $\mu_x^{\rm ml}$ (i.e., the chemical potential at point 3 in figure 1), a *truly* equilibrated system changes from monolayer to the (now globally stable) liquid phase (the associated discontinuity in $\bar{\rho}$ is indicated in figure 1 by the dotted line connecting points 3). However, in the typical finite-time experiment, it is most likely that the monolayer persists as a metastable state until μ considerably exceeds $\mu_x^{\rm ml}$. Only at the monolayer's spinodal (point b in figures 1 and 2) must the monolayer undergo a transformation into a thermodynamically stable liquid phase.

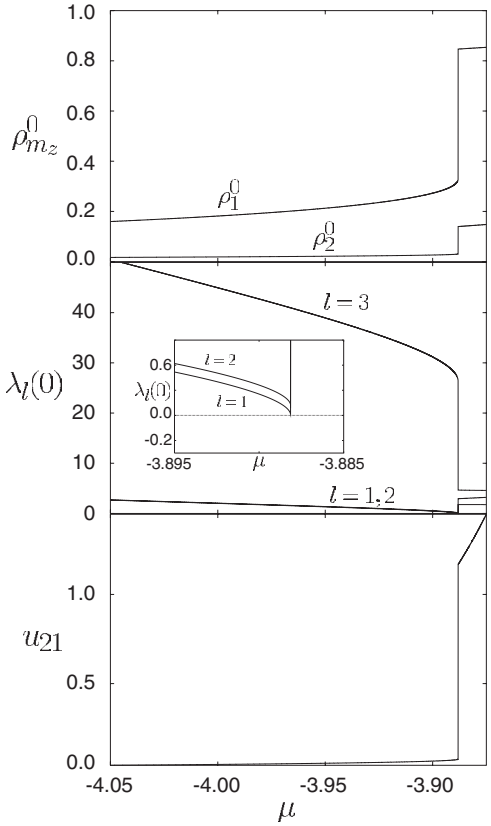

Figure 3. Local densities $\rho^0_{m_z}$, eigenvalues $\lambda_l(0)$ of the reciprocal-space Hessian at $\boldsymbol{k} = \mathbf{0}$, and mid-plane component of the dominant mode versus μ over the range of existence of the gas for $n_z = 3$, $\epsilon_{\rm fw} = 1.9$, and $T = 0.9$.

The approach to the monolayer's stability limit is quantified in figure 4, where we see that $\lambda_1(0)$ goes to zero and that $u_{21} \gg 1$. The latter implies that the mid-plane component of the dominant mode greatly exceeds those of the contact planes, which is consistent with the observation that the shift in local density is greatest in the mid-plane (see the top plot in figure 4). Finally, as μ increases from point b, the liquid phase remains stable up to the end point 4 (see figures 1 and 2).

We now consider the phase behaviour of the system as we reverse the 'direction' of the experiment by gradually *lowering* μ from point 4, where ω has only a single minimum corresponding to the stable liquid phase. If thermodynamic equilibrium were attained at all values of μ (which means, in principle, waiting for an infinite time), the path followed by the system in the sorption diagram (see figure 1) would clearly be $4 \to 3 \to 2 \to 1$. However, since the experiment is conducted over a finite period, the system may not achieve equilibrium at all values of μ. This gives rise to the hysteresis loops in figure 1. For example, as μ drops below the value corresponding to point 3 (i.e., the point of liquid–monolayer coexistence), the system may remain in the now metastable liquid phase until its limit of stability is reached at point c. Similarly, as μ decreases below the value corresponding to point c, the monolayer phase, which is globally stable down to $\mu_x^{\rm gm}$ (point 2), may persist as a metastable phase until point d is reached. The precise behaviour of the system as the spinodal points c and

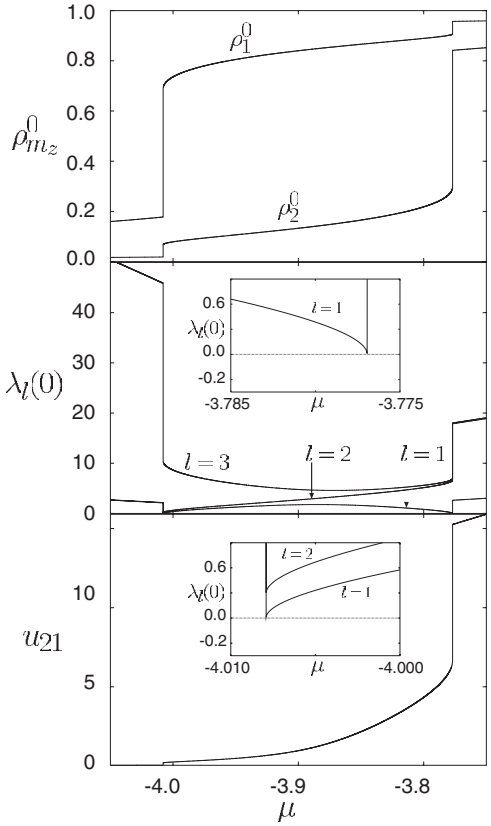

Figure 4. As figure 3, but for the monolayer phase.

d are approached 'from above' is quantified in figures 4 and 5, respectively. In both cases, the approach to the spinodal is signalled by the vanishing of $\lambda_1(0)$. Furthermore, $u_{21} \gg 1$ when the system changes from liquid to monolayer (see figure 5), whereas $u_{21} \ll 1$ for the final change from monolayer to gas (see figure 4). These observations are consistent with the behaviour of the local densities (see the top plots in figures 4 and 5, showing that the largest jump in local density occurs in the mid-plane at spinodal c and in the contact planes at spinodal d). We conclude that the eigenvector corresponding to the dominant vanishing eigenvalue indicates the physical nature of the incipient phase.

Repeating the above *gedanken* experiment at other temperatures permits us to plot the complete phase diagram of the three-layer system ($\epsilon_{\mathrm{fw}} = 1.9$) in both $\bar{\rho}$–T and μ–T representations in figures 6(a) and (b), respectively. The solid lines connect points of two-phase coexistence; the dotted lines represent the stability limits of gas, monolayer, and liquid phases over the temperature range where these phases *may* become thermodynamically stable. (Therefore, spinodals referring to the monolayer terminate at the triple-point temperature.) In order to understand the sorption 'path' discussed above in the $\bar{\rho}$–T diagram (see figure 6(a)), consider again the temperature $T = 0.9$. As μ increases from point 1 a state is reached in which the gas coexists with the monolayer (point 2). However, the gas may remain metastable for μ corresponding to states between the points 2 and a. At point a the gas becomes unstable and transforms into a monolayer. Note that the average density of the monolayer is *higher* than at

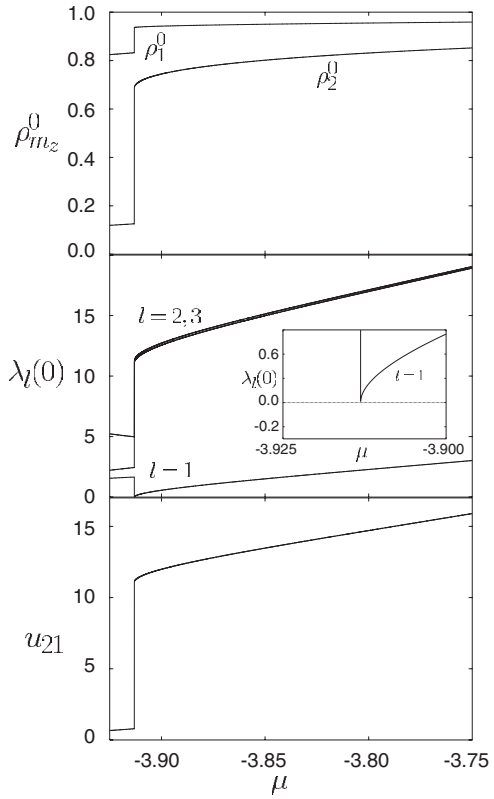

Figure 5. As figure 3, but for the liquid phase.

coexistence with the gas (see point 2, figure 1). As μ increases beyond point 3, the monolayer may not undergo a phase transition to the coexisting liquid, but may remain metastable until the next spinodal is reached (point b). At point b the monolayer becomes unstable and a liquid phase forms. Its density is intermediate between the one at monolayer–liquid coexistence (point 3) and that of the stable liquid (see point 4, figure 1). Similar considerations apply if we start at state point 4 and decrease μ continuously. Note that upon adsorption (i.e., as μ increases in the direction $1 \rightarrow 4$), spinodals on which points d and c are located have no physical significance. Likewise spinodals on which points b and a reside are irrelevant upon *de*sorption (path $4 \rightarrow 1$).

It is furthermore instructive to consider the phase diagram in the alternative μ–T representation in figure 6(*b*). Again, the dotted lines containing points a and b (c and d) are the spinodals that the (metastable) state of the system can reach upon adsorption (desorption). It can be verified that the μ–T diagram is consistent with our discussion of the sorption paths (see figure 1). For instance, figure 6(*b*) shows that the chemical potential (and the temperature) corresponding to point a, at which the (metastable) gas becomes unstable for $T = 0.9$ (see figure 1), belongs to the one-phase region of the monolayer. This implies, in accord with the preceding discussion, that the metastable gas transforms into a globally stable monolayer for μ beyond gas–monolayer coexistence (point 2).

Moreover, the μ–T diagram shows directly that the destiny of the metastable gas upon adsorption changes at lower temperatures. Consider, for example, the isotherm $T = 0.8$, for

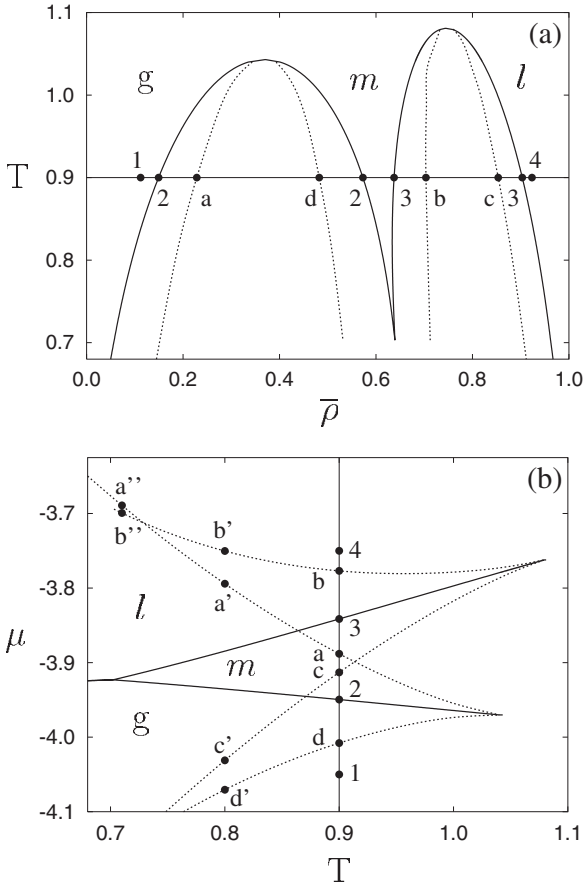

Figure 6. Phase diagrams for the model slit-pore with chemically homogeneous walls in T–ρ (a) and μ–T (b) representations, for $n_z = 3$ and $\epsilon_{\rm fw} = 1.9$. The isotherms are explained in the text.

which μ at the spinodal of the (metastable) gas phase (point a′) now exceeds μ at monolayer–liquid coexistence (in contrast to the situation for $T = 0.9$). In other words, a′ does not belong to the one-phase region of thermodynamically stable monolayer phases, while on the other hand, μ at point a′ is still lower than μ where the (metastable) monolayer reaches its limit of stability (point b′). For an adsorption experiment this implies that the metastable gas again transforms into a monolayer (as at $T = 0.9$), but now this monolayer is *metastable*. As μ increases from a′, the metastable monolayer eventually transforms (at point b′) into (globally) stable liquid. The various states appearing along this path can also be seen from the corresponding sorption isotherm plotted in figure 7(a).

At $T = 0.8$, an inspection of u_{21} versus μ for the metastable gas indicates that $u_{21} \ll 1$ at the spinodal (point a′), similar to the case for the corresponding plot for $T = 0.9$ in the bottom panel of figure 3. Likewise, $u_{21} \gg 1$ at the monolayer's spinodal (point b′). At the spinodals c′ and d′ on the reverse path, where metastable liquid transforms to metastable monolayer and metastable monolayer to stable gas, respectively, $u_{21} \gg 1$ and $u_{21} \ll 1$. Therefore, the amplitude of the mid-plane component of the dominant (softest) mode does indeed indicate reliably the nascent phase. However, that the newly formed monolayer is merely *metastable* can be determined only from a knowledge of the complete phase diagram.

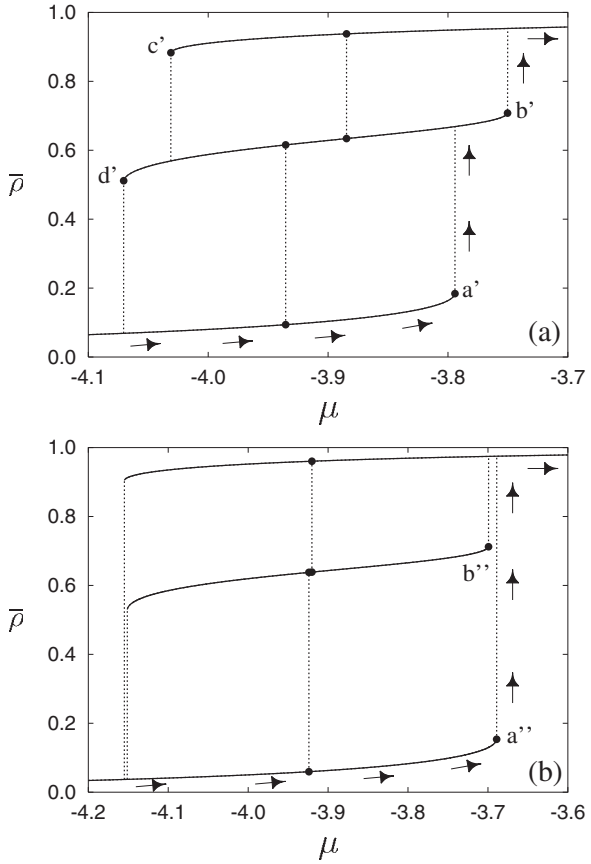

Figure 7. As figure 1, but for $T = 0.80$ (*a*) and $T = 0.71$ (*b*).

Yet another qualitative change in the fate of the metastable gas occurs at even lower temperatures, in the vicinity of the intersection of the spinodals in the μ–T representation (see figure 6(*b*)). As an example we consider $T = 0.71$, which is slightly above the triple-point temperature $T_{\rm tr} \simeq 0.703$. It can be seen that μ at point a″, at which the gas becomes unstable, is now *larger* than μ at the monolayer's spinodal (point b″). Thus, as μ increases from a value below b″, the metastable gas transforms *directly* into a (globally) stable liquid (see also figure 7(*b*)). In other words, the monolayer does not participate at all in the phase transformation at $T = 0.71$.

At $T = 0.71$, an inspection of u_{21} versus μ reveals that $u_{21} \ll 1$ at the spinodal (point a″) of the metastable gas. This suggests that the incipient phase is the metastable monolayer. However, we know that μ at point a″ exceeds μ at the stability limit (point b″) of the monolayer. It is clear, therefore, that the inference based on the dominant eigenvector is misleading in this case. Additional numerical studies show that the dependence of $\rho^0_{m_z}$ on μ over the range of existence of the metastable gas, as indicated in the top panel of figure 3, does not change as strongly with temperature for $T > T_{\rm tr}$. Thus, we expect the inequality $u_{21} \ll 1$ to hold over this range. That is, we expect the dominant eigenvector to signal correctly the monolayer (either stable or metastable) as the destination of the metastable gas over the range of the latter's existence, at least *above* the temperature where the stability-limit lines (a and b) intersect (see figure 6(*b*)).

5. Summary and conclusions

In the present paper we investigate the role of metastable states involved in first-order phase transformations of a fluid confined to a nanoscopic slit-pore. Following previous investigations [9] we model the system as a lattice gas with nearest-neighbour interactions. Thermodynamic properties are calculated within the grand canonical ensemble, where temperature (T), chemical potential (μ), and the distance (n_z) between the walls are controlled variables. The best estimate for the grand potential Ω is obtained by minimizing the grand potential functional $\Omega[\boldsymbol{\rho}]$ of the local densities $\boldsymbol{\rho} = \{\rho_i, i = 1, \ldots, \mathcal{N}\}$, where $\mathcal{N}$ is the number of lattice sites. The mean-field approximation is used to evaluate the interaction contribution to $\Omega[\boldsymbol{\rho}]$.

A central goal of our work is to develop a formalism for determining the limits of existence of the various metastable states of the confined system (i.e. the so-called 'spinodals'). The starting point is the idea that in a stable or metastable state (i.e., at a *minimum* of the grand potential functional $\Omega[\boldsymbol{\rho}]$), small displacements of the local densities from their values ρ_i^0 at the minimum lead to an increase $\delta\Omega$ in Ω. We estimate this 'cost' $\delta\Omega$ by expanding the density functional up to second order in the displacements $\delta\rho_i = \rho_i - \rho_i^0$. This yields a quadratic expression in $\delta\rho_i$ for $\delta\Omega$, where the associated expansion coefficients are elements of the Hessian matrix $H_{ij} = (\partial^2\Omega/\partial\rho_i\,\partial\rho_j)_0$. The matrix $\mathbf{H}$ comprises an entropic contribution, given explicitly in terms of T and the densities ρ_i^0, as well as an interaction contribution which generally takes the form of a state-dependent direct correlation function. In the mean-field approximation, however, the direct correlation function is just the (state-independent) pair potential, in which case knowledge of the densities alone is sufficient for calculating the Hessian. Stability of a given state requires that all eigenvalues of the $\mathcal{N} \times \mathcal{N}$ Hessian matrix be positive. The eigenvalues can be interpreted as 'force constants' measuring the resistance of the system to certain *collective* density displacements, the direction of which (in density space) is determined by the eigenvectors of the Hessian. As a metastable state approaches its stability limit (i.e., a spinodal), certain eigenvalues go to zero, indicating that the corresponding normal modes are 'softening'. The direction of the soft modes in density space can provide information about the character of the phase beyond the spinodal.

The stability criteria outlined in section 3.1 are general in the sense that they apply to any (confined) lattice gas with arbitrarily complex walls, and also for any approximation to the interaction contribution to $\Omega[\boldsymbol{\rho}]$. However, direct diagonalization of the real-space Hessian matrix is out of question for large $\mathcal{N}$. Indeed, the method is practicable only if the equilibrium states of the system possess spatial symmetries, for example *full* translational symmetry in planes parallel with the walls (as for a system with chemically homogeneous walls). In section 3.2 we show how to exploit this symmetry by means of a two-dimensional discrete Fourier transform. Thereby, $\delta\Omega$ decouples into independent contributions from different discrete wavevectors $\boldsymbol{k}$, and the stability criteria can be formulated in terms of the $\boldsymbol{k}$-dependent eigenvalues of the $n_z \times n_z$ reciprocal-space Hessian $\tilde{\mathbf{H}}(\boldsymbol{k})$. The problem of determining the eigenvalues of the original $\mathcal{N} \times \mathcal{N}$ matrix $\mathbf{H}$ thus reduces to that of diagonalizing relatively small matrices.

As demonstrated in section 3.3, additional decouplings in $\tilde{\mathbf{H}}(\boldsymbol{k})$ arise from the mean-field approximation, combined with the nearest-neighbour restriction on the pair potential. Incorporating these assumptions, we show that the eigenvalues can go to zero *only* in the long-wavelength limit (i.e. at $\boldsymbol{k} = \mathbf{0}$). This implies that collective density fluctuations against which the system becomes unstable at the spinodals are homogeneous within the lattice planes.

A further implication of vanishing $\boldsymbol{k} = \mathbf{0}$ eigenvalues is discussed in section 3.4, where we derive (*in principle*) exact relations between the eigenvalues and eigenvectors of $\tilde{\mathbf{H}}(\boldsymbol{k})$ and the matrix $\tilde{\mathbf{G}}(\boldsymbol{k})$ containing density–density correlations within and between the lattice planes.

Expanding the eigenvalues around $\boldsymbol{k} = \mathbf{0}$ enables us to examine the long-range behaviour of the corresponding *real-space* correlations. Within the present approximations and under the assumption that the system is still (meta)stable, the asymptotic behaviour of the correlation functions can be cast in a closed form, namely as a sum of exponentials $\exp(-R/\xi_l)/\sqrt{R}$, where the n_z-correlation lengths ξ_l are essentially the inverse eigenvalues of $\tilde{\mathbf{H}}(\boldsymbol{k})$ at $\boldsymbol{k} = \mathbf{0}$. Consequently, a decrease of a certain eigenvalue yields an increasing correlation length, which is precisely what one expects in the vicinity of a phase transition. From a more technical viewpoint, it is interesting that the above exponential decay in the correlations of a confined, but still fully three-dimensional, fluid agrees with the Ornstein–Zernike result for a correlation function in a *true* two-dimensional system [28].

Finally in section 4 we illustrate our approach by considering a confined system with homogeneous walls and $n_z = 3$, for which the Hessian can be diagonalized analytically. For an appropriately chosen fluid–wall interaction, the equilibrium μ–T phase diagram reveals the existence of three morphologically distinct stable phases above a triple temperature T_{tr}. Regions where these states are only metastable overlap and the relative locations of spinodals and phase coexistence lines vary with temperature. Focusing on three particularly interesting isothermal paths, we perform an analysis of the $n_z = 3$ eigenvalues and eigenvectors characterizing the (meta)stable states. In addition, we delineate the μ-dependence of sorption isotherms, which are directly measurable in parallel sorption experiments. The sorption isotherms exhibit relatively wide hysteresis loops, indicating 'pathways' that the system may take in an experiment performed on a *finite* timescale. The 'new' phase to which a metastable phase decays upon approaching its spinodal does not always coincide with the globally stable state. Under certain conditions the transformation between two globally stable phases involves another intermediate metastable phase. The lifetime of such a metastable phase could be quite long compared to the equilibration time available in a finite-time laboratory experiment. Thus, the relative stability of, and reproducibility of occurrence of such a metastable phase may lead the experimenter to believe that the newly formed phase is a globally stable one. From this we conclude that there is a real worry about the significance of experimentally determined phase diagrams of fluids in porous media, even in cases where the pore geometry is relatively simple. Furthermore, close to T_{tr}, the stable phase appearing at intermediate μ can actually be pre-empted by driving the low-μ state to its spinodal.

With the exception of the last phenomenon, which is specific to the vicinity of the triple point, the 'destiny' of the metastable states is well reflected by the character of the soft modes (i.e., the dominant fluctuations) close to the spinodal. In other words, the eigenvector associated with the vanishing eigenvalue has the 'right direction' in the sense that the diverging density fluctuations already have the character of the new phase beyond the spinodal. Therefore, the dominant eigenmodes appear to be a reliable indicator of the new phase to which the metastable phase decays. In the light of this experience we expect the stability analysis to work also for other fluid–wall interaction strengths, or for thicker systems (i.e. larger n_z), where the diagonalization of $\mathbf{H}$ can only be carried out numerically.

The analysis of metastable states presented here could also be a useful tool for investigating the phase behaviour of more complex systems with less spatial symmetry (compared to the full in-plane symmetry for the case of homogeneous walls). An example would be a fluid confined by chemically 'striped' walls, the equilibrium states of which [8,9] are symmetric with respect to one of the two spatial directions parallel to the walls. In the context of a stability analysis, this remaining symmetry could be exploited by means of a one-dimensional discrete Fourier transform. This would give rise to an $(M \times n_z) \times (M \times n_z)$ matrix $\tilde{\mathbf{H}}(\boldsymbol{k})$, where M is the period of the stripes. Although the matrix is larger than the smooth-wall one, it is nevertheless substantially smaller than the original real-space $\mathbf{H}$.

Acknowledgments

We are pleased to acknowledge stimulating discussions with Professor G Tarjus (Université Pierre et Marie Curie). We are also grateful for support from the Sonderforschungsbereich 448 'Mesoskopisch strukturierte Verbundsysteme'. SHLK acknowledges financial support from the Deutsche Forschungsgemeinschaft through the Emmy Noether programme. DJD thanks the Alexander von Humboldt Foundation for the generous Research Award that made possible an extended stay in Germany. He is also grateful to Professors G H Findenegg and S Hess for their cordial hospitality.

Appendix A. Discrete Fourier transform

Let $f(\boldsymbol{R})$ be specified on the M^2 sites of a square lattice and let the sites be labelled from $m_\alpha = -M/2+1$ to $M/2$ ($\alpha = x, y$), where for convenience M is taken to be even. We define a complete, orthonormal set of basis vectors $\Psi_k(\boldsymbol{R})$ that span the M^2 sites:

$$\Psi_k(\boldsymbol{R}) \equiv \frac{1}{M}\exp\left(\frac{2\pi \mathrm{i}\boldsymbol{k}\cdot\boldsymbol{R}}{M}\right) \qquad -\frac{M}{2} < k_x, k_y \leqslant \frac{M}{2} \tag{A.1}$$

where $\mathrm{i} \equiv \sqrt{-1}$ and the '$<$' for the first part of the inequality signifies that $k_\alpha \geqslant -M/2+1$. In (A.1), $\boldsymbol{R}$ and $\boldsymbol{k}$ represent vectors with integer components $\boldsymbol{R} = (m_x, m_y)$ and $\boldsymbol{k} = (k_x, k_y)$. It may be shown that [30]

$$\sum_{\boldsymbol{R}} \Psi_{\boldsymbol{k}}^*(\boldsymbol{R})\Psi_{\boldsymbol{k}'}(\boldsymbol{R}) = \delta_{\boldsymbol{k},\boldsymbol{k}'} \tag{A.2}$$

$$\sum_{\boldsymbol{k}} \Psi_{\boldsymbol{k}}^*(\boldsymbol{R})\Psi_{\boldsymbol{k}}(\boldsymbol{R}') = \delta_{\boldsymbol{R},\boldsymbol{R}'} \tag{A.3}$$

where the superscript '$*$' denotes the complex conjugate. Since the Ψ_k span the M^2 lattice sites, any function $f(\boldsymbol{R})$ given on those sites can be expressed as a linear combination of the $\{\Psi_k\}$:

$$f(\boldsymbol{R}) = \sum_{\boldsymbol{k}} \tilde{f}(\boldsymbol{k})\Psi_{\boldsymbol{k}}(\boldsymbol{R}). \tag{A.4}$$

The coefficients $\tilde{f}(\boldsymbol{k})$ can be determined by multiplying (A.4) by $\Psi_{\boldsymbol{k}'}^*(\boldsymbol{R})$, summing on $\boldsymbol{R}$, and invoking the relation in (A.2). The result is

$$\tilde{f}(\boldsymbol{k}) = \sum_{\boldsymbol{R}} f(\boldsymbol{R})\Psi_{\boldsymbol{k}}^*(\boldsymbol{R}). \tag{A.5}$$

Together $f(\boldsymbol{R})$ and $\tilde{f}(\boldsymbol{k})$ constitute the discrete Fourier transform pair: f is the representation of the function in real ($\boldsymbol{R}$) space; $\tilde{f}$ is its representation in reciprocal ($\boldsymbol{k}$) space.

Note that we may 'partially' transform a function defined on a 3D cubic lattice to 2D reciprocal space. Thus, consider a function $f(\boldsymbol{R}, m_z)$ on the 3D lattice. We expand f in the 2D basis vectors as

$$f(\boldsymbol{R}, m_z) = \sum_{\boldsymbol{k}} \tilde{f}(\boldsymbol{k}, m_z)\Psi_{\boldsymbol{k}}(\boldsymbol{R}) \tag{A.6}$$

where the argument m_z reminds us that $\tilde{f}$ implicitly depends on the z-coordinate of the lattice plane. Following the reasoning that leads from (A.4) to (A.5), we arrive at

$$\tilde{f}(\boldsymbol{k}, m_z) = \sum_{\boldsymbol{R}} f(\boldsymbol{R}, m_z)\Psi_{\boldsymbol{k}}^*(\boldsymbol{R}). \tag{A.7}$$

Taking $f(\boldsymbol{R}, m_z)$ to be real, we have from (A.7)

$$\tilde{f}^*(\boldsymbol{k}, m_z) = \sum_{\boldsymbol{R}} f(\boldsymbol{R}, m_z)\Psi_{\boldsymbol{k}}(\boldsymbol{R}) = \tilde{f}(-\boldsymbol{k}, m_z) \tag{A.8}$$

where the third branch of the equality follows from (A.1).

It follows from (A.5) that $\delta_{\boldsymbol{R},\boldsymbol{R}'}$ is represented in reciprocal space by

$$\tilde{\delta}_{\boldsymbol{R},\boldsymbol{R}'}(\boldsymbol{k}) = \sum_{\boldsymbol{R}-\boldsymbol{R}'} \delta_{\boldsymbol{R},\boldsymbol{R}'}\Psi^*_{\boldsymbol{k}}(\boldsymbol{R}-\boldsymbol{R}') = \Psi^*_{\boldsymbol{k}}(\boldsymbol{0}) = \frac{1}{M}. \tag{A.9}$$

By similar reasoning, we can derive the relation

$$\tilde{\delta}_{\boldsymbol{R}-\boldsymbol{R}',\hat{\boldsymbol{d}}_\parallel}(\boldsymbol{k}) = \frac{1}{M}\exp\left(-\frac{2\pi \mathrm{i}\boldsymbol{k}\cdot\hat{\boldsymbol{d}}_\parallel}{M}\right). \tag{A.10}$$

Appendix B. Asymptotic analysis of (3.44)

The purpose of this appendix is to evaluate the integral in (3.44) approximately in closed form and to examine its asymptotic dependence on R. We assume that $\lambda_l(0) > 0$.

Making the substitution

$$x = \kappa R \tag{B.1}$$

we can rewrite (3.44) as

$$\eta_l(R) = \frac{1}{4\pi^2\beta}\int_0^{2\pi} \mathrm{d}\varphi \int_0^{R\kappa(\varphi)} \mathrm{d}x\, \frac{x\exp(\mathrm{i}x\cos\varphi)}{\lambda_l(0)R^2 + x^2}. \tag{B.2}$$

We now suppose that R becomes sufficiently large that the upper limit of the κ-integral in (B.2) can be taken to infinity without incurring significant error. Using that the real (imaginary) part of the integrand is even (odd) in the interval $[0, 2\pi]$ and the identity $\int_0^\pi \mathrm{d}\varphi \cos(x\cos\varphi) = \pi J_0(x)$ [31], where $J_0(x)$ is the zeroth-order Bessel function, we can perform the φ-integration in (B.2) to obtain

$$\eta_l(R) = \frac{1}{2\pi\beta}\int_0^\infty \mathrm{d}x\, \frac{xJ_0(x)}{\lambda_l(0)R^2 + x^2}. \tag{B.3}$$

The remaining definite integral in (B.3) is given by Gradshteyn and Ryzhik [32] as

$$\eta_l(R) = \frac{1}{2\pi\beta}K_0(R/\xi_l) \tag{B.4}$$

where we defined the 'correlation length'

$$\xi_l \equiv \frac{1}{\sqrt{\lambda_l(0)}} \tag{B.5}$$

and $K_0(z)$ is the Bessel function of imaginary argument, which is given in terms of the zero-order Hankel function of the first kind $H_0^{(1)}$ by [33]

$$K_0(z) = \frac{\pi\mathrm{i}}{2}H_0^{(1)}(\mathrm{i}z). \tag{B.6}$$

The asymptotic dependence of $H_0^{(1)}(z)$, where z is complex, is given by Abramowitz and Stegun [34] as

$$\lim_{z\to\infty} H_0^{(1)}(z) \sim \sqrt{\frac{2}{\pi z}}\exp\left[\mathrm{i}\left(z - \frac{\pi}{4}\right)\right] \qquad -\pi < \arg z < 2\pi. \tag{B.7}$$

In the present case, the argument of K_0, $z = R/\xi_l$, is real, so, combining (B.6) and (B.7), we find

$$\lim_{R\to\infty} K_0(R/\xi_l) = \frac{\pi \mathrm{i}}{2}\sqrt{\frac{2\xi_l}{\pi \mathrm{i} R}}\exp\left[\mathrm{i}\left(\frac{\mathrm{i}R}{\xi_l} - \frac{\pi}{4}\right)\right] = \sqrt{\frac{\pi\xi_l}{2R}}\exp(-R/\xi_l) \quad \text{(B.8)}$$

where we used that $\exp(-\mathrm{i}\pi/4) = 1/\sqrt{\mathrm{i}}$. Combining (B.4) and (B.8) we finally obtain the result (3.45).

References

[1] Balian R 1991 *From Microphysics to Macrophysics. Methods and Applications of Statistical Physics* vol 1 (Berlin: Springer)
[2] Frenkel J 1946 *Kinetic Theory of Liquids* (Oxford: Clarendon) ch VII
[3] Langer J S 1969 *Ann. Phys., NY* **54** 258
[4] Gunton J D, San Miguel M and Sahni P S 1983 *Phase Transitions and Critical Phenomena* ed C Domb and J L Lebowitz (London: Academic) p 267
[5] Schoen M and Diestler D J 1997 *Chem. Phys. Lett.* **270** 339
[6] Schoen M and Diestler D J 1997 *Phys. Rev.* E **56** 4427
[7] Bock H and Schoen M 1999 *Phys. Rev.* E **59** 4122
[8] Bock H and Schoen M 2000 *J. Phys.: Condens. Matter* **12** 1569
[9] Bock H, Diestler D J and Schoen M 2001 *J. Phys.: Condens. Matter* **13** 4697
[10] Bock H, Diestler D J and Schoen M 2001 *Phys. Rev.* E **64** 046124-1
[11] Bock H, Schreiber A, Findenegg G H and Schoen M 2002 *Mol. Phys.* at press
[12] Crassous J, Charlaix E and Loubet J 1994 *Europhys. Lett.* **28** 37
[13] Turnbull D 1950 *J. Chem. Phys.* **18** 198
[14] Oxtoby D W 1992 *Fundamentals of Inhomogeneous Fluids* ed D Henderson (New York: Dekker) p 407
[15] Yasuoka K, Gao G T and Zeng X C 2000 *J. Chem. Phys.* **112** 4279
[16] Restagno F, Bocquet L and Biben T 2000 *Phys. Rev. Lett.* **84** 2433
[17] Talanguer V and Oxtoby D W 2001 *J. Chem. Phys.* **114** 2793
[18] Lavis D A and Bell G M 1999 *Closed-Form and Exact Solutions (Statistical Mechanics of Lattice Systems vol 1)* 2nd edn (Berlin: Springer) ch 5
[19] Hill T L 1986 *An Introduction to Statistical Thermodynamics* (New York: Dover) ch 7
[20] Callen H B 1985 *Thermodynamics and an Introduction to Thermostatics* 2nd edn (New York: Wiley) ch 20
[21] Ruelle D 1999 *Statistical Mechanics. Rigorous Results* (Singapore: World Scientific) p 130
[22] Chen X S, Kasch M and Forstmann F 1991 *Phys. Rev. Lett.* **67** 2674
[23] Chen X S and Forstmann F 1992 *Mol. Phys.* **76** 1203
[24] Klapp S and Forstmann F 1997 *J. Chem. Phys.* **106** 9742
[25] Ornstein L S and Zernike F 1914 *Proc. Akad. Sci. (Amsterdam)* **17** 793
[26] Hansen J-P and McDonald I R 1976 *Theory of Simple Liquids* 1st edn (London: Academic) ch 10.2
[27] Morandi G, Napoli F and Ercolesi E 2001 *Statistical Mechanics. An Intermediate Course* 2nd edn (Singapore: World Scientific) ch 7.1.5
[28] Stanley H E 1971 *Introduction to Phase Transitions and Critical Phenomena* (Oxford: Oxford University Press) ch 7
[29] Fisher M E 1962 *Physica* **28** 172
[30] Arfken G 1985 *Mathematical Methods for Physicists* (London: Academic) ch 14
[31] Abramowitz M and Stegun I R 1965 *Handbook of Mathematical Functions (NBS, Applied Mathematical Series 55)* (Washington, DC: US Government Printing Office) p 360
[32] Gradshteyn I S and Ryzhik I M 1980 *Table of Integrals, Series, and Products* (New York: Academic) p 678
[33] Gradshteyn I S and Ryzhik I M 1980 *Table of Integrals, Series, and Products* (New York: Academic) p 952
[34] Abramowitz M and Stegun I R 1965 *Handbook of Mathematical Functions (NBS, Applied Mathematical Series 55)* (Washington, DC: US Government Printing Office) p 364